DYNAMIC MODELING OF A SILICON BULK-MICROMACHINED MICROACCELEROMETER

JANDERSON R. RODRIGUES[1,2], LUIZ C. S. GOES[1], ANGELO PASSARO[2], CARLOS F. R. MATEUS[2].

1. *Aeronautics and Mechanical Engineering, Aeronautics Institute of Technology (ITA)*
ZIP CODE 12228-900, São José dos Campos – SP – Brazil

2. *Applied Physics Division, Institute for Advanced Studies(IEAv)*
ZIP CODE, 12228-001, São José dos Campos – SP – Brazil
E-mails: jrr@ita.br, goes@ita.br, angelo@ieav.cta.br

Abstract— In this work, we describe dynamic modeling and simulation of a capacitive silicon bulk-micromachined microaccelerometer. The modeling of the mechanical part is done through equivalent stiffness and equivalent damping coefficients analyses using the Euler-Bernoulli equation and the Modified Reynolds equation, respectively. A dynamic model is obtained taking into account the electric force influence between the electrodes. Nonlinear and linear models are compared. The analytical results are compared with numerical results obtained by computational method in both time-domain and frequency-domain and it show a quite good agreement.

Keywords— Microaccelerometer, MEMS, Modeling, Dynamic, Sensor.

1 Introduction

The increasing demand in new applications has driven research and continuous development of MEMS devices. This is the case, for instance, of micro-accelerometers and micro-gyroscopes for aerospace applications, as part of inertial measurement units (IMU's).

For aerospace applications these devices must present high-level specification. In order to achieve these specifications, it is necessary to consider the interactions between the various physics domains involved in microsystems modeling, MNX (2008).

One of these interactions is between the moving mechanical components and the fluid surrounding them, what makes possible to find out the exact dynamic behavior of the structure. Once the main damping mechanism is known, it allows us to get the desired frequency response of the micro device by controlling the fluid pressure, viscosity coefficient or the gap layer, Veijola *et. al*. (1995).

This work describes analysis of a microaccelerometer. This accelerometer is fabricated by bulk micromachining of silicon in KOH solution. The mechanical part of this device consists of an inertial mass suspended by four silicon beams fixed at the edges. The calculation of the equivalent stiffness coefficients are done using basic solid mechanics theory. Both large and small deflections cases are analyzed in this study.

We determined the Young's modulus according to the crystallographic orientation of the silicon beams. The calculation of the mass and the second moment of area is done taking into account the hexagonal cross section formed during the bulk-micromachined process. The effective mass of the system is calculated discussing the influence of the mass of beams.

We describe the behavior of the gas between the electrodes with the modified Reynolds equation. Both large and small displacement cases are analyzed. The nonlinear and linear dynamic models are compared. The validity of the analytical model is discussed according to the assumptions and simplifications made. Finally, all analytical results are compared with numerical results obtained by Computational Fluid Dynamics method (CFD) in both time-domain and frequency-domain. The results show very good agreement between the two methods, validating the analytical model for this kind of analysis.

2 Microaccelerometer Model

The bulk-micromachined accelerometer simulated consists of a stack of three bonded silicon wafers, with the hinge springs and seismic mass incorporated in the middle one. The inertial mass forms a moveable inner electrode of a variable differential capacitor circuit, show in Fig 1. The two outer identical wafers are simply the fixed electrodes of the two capacitors. The differential capacitor senses the relative position of the inertial mass as it displaces under the effect of an externally applied acceleration. Electronic circuit sense changes in capacitance, then convert them into an output voltage.

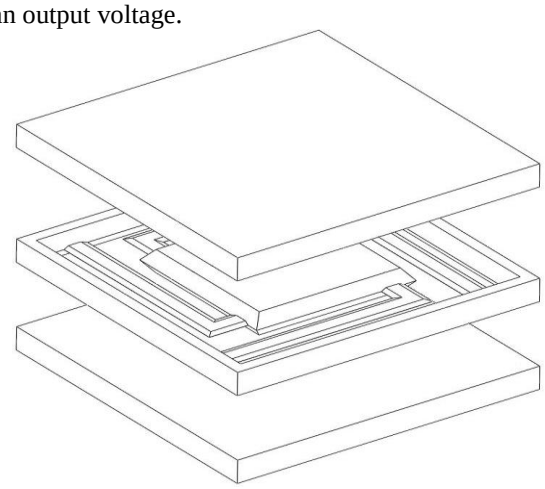

Figure 1. 3D views of the accelerometer.

DOI: 10.5540/03.2013.001.01.0140

The geometric parameters of such device are presented in Table 1. The data correspond to the values defined previously in the accelerometer design.

Table 1. Some geometric parameters of the accelerometer.

Description	Symbol	Value [μm]
Length of the seismic mass	L_m	2000
Width of the seismic mass	W_m	2000
Thickness of the seismic mass	T_m	380
Length of the beam	l_b	2820
Width of the beam	w_b	177
Thickness of the beam	t_b	55
Gap between the silicon wafers	h_o	5

In summary, the microfabrication of a bulk accelerometer involves a sequence of processes, e.g. thin film deposition, double face lithography, simultaneous top and bottom wet etching, bonding of the three wafers.

The wet etching makes use of potassium hydroxide aqueous solution, known as KOH solution. Both sides of the middle wafer are etched, forming the seismic mass suspended by four beams. The KOH solution etches the monocrystalline silicon anisotropically, i.e., with different etching rate, according to the orientation of the silicon's crystal planes, (Dziuban, 2006). Due to this characteristic, after etching, the geometry of the device has a slightly different format from de one designed in the photolithography mask. The KOH etching process results in beams and seismic mass with an irregular hexagon cross-sectional area, Fig. 2.

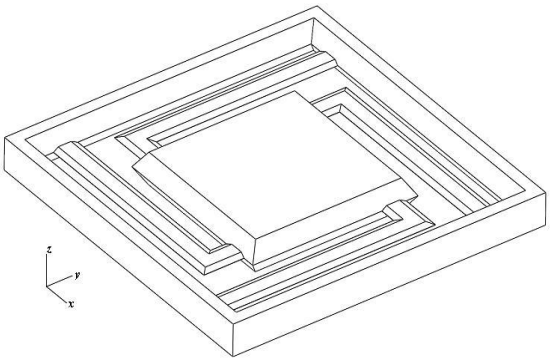

Figure 2. 3D view of middle wafer after KOH etching.

The seismic mass has a form of two truncated pyramids with square base mounted in the opposite way. This format is defined by the (100) plane at the top, and bottom, surrounded by the (111) plane. The angle between the seismic mass' top plane and the seismic mass' edges is 54.74º. The thicknesses of seismic mass and the edges are the same as the original thickness of the wafers.

The thickness of the beams is defined during the KOH etching, with the removal of the mask and the formation of high-index planes. The format of the beams is set with (100) plane at the top, and bottom, surrounded by a high-index (411) plane formatting an irregular hexagon. The angle between the beam's top plane and the beam's edges is 19.57°, (Dziuban, 2006).

3 Analytical approach

3.1. Equivalent stiffness coefficient for Small and Large Deflection

The equivalent stiffness coefficient of the accelerometer can be obtained by using the Euler-Bernoulli equation. The accelerometer model can be decomposed into two parallel clamped-clamped beam subjected to a concentrated load at the seismic mass. In the case of small deflections it results in a linear relation between the load F_z and the deflection δ_z, with the equivalent stiffness given by (Beer *et al.* 2006),

$$k_{eq} = \frac{48EI}{{l_b}^3} \tag{1}$$

where E is the Young's Modulus and I is the Second Moment of Area.

In the case of large deflections, the analysis has to include the longitudinal axial force N that develops inside the beams. This axial force results in a nonlinear relation between the load and the deflection that can be founded by simultaneously solving the next set of equations, (Legtenberg *et al.*, 1996):

$$F_z(u) = \frac{EIt_b}{{l_b}^3}\sqrt{\frac{8}{3}}u^3\left(\frac{3}{2} - \frac{1}{2}\tanh^2 u - \frac{3}{2}\frac{\tanh u}{u}\right)^{-\frac{1}{2}} \tag{2}$$

$$\delta_z(u) = t_b\sqrt{\frac{2}{3}}(u - \tanh u)\left(\frac{3}{2} - \frac{1}{2}\tanh^2 u - \frac{3}{2}\frac{\tanh u}{u}\right)^{-\frac{1}{2}} \tag{3}$$

with

$$u = \frac{l_b}{2}\sqrt{\frac{N}{EI}} \tag{4}$$

where u is the common variable and depends on the axial force N. The equivalent nonlinear stiffness coefficient of two parallel clamped-clamped beam is obtained doing $F_z/2$ in Eq. (2). Due to this nonlinearity when the deflection increases the stiffness coefficient of the beam becomes much larger than in the linear case.

3.2. Young's Modulus

Monocrystalline silicon is an anisotropic crystal therefore its mechanical properties vary with respect

to crystallographic direction. The Young's modulus for an arbitrary crystallographic direction l is given by, Brantley (1973),

$$E_{[l_1,l_2,l_3]} = \{S_{11} - 2(S_{11} - S_{12} - 1/2\,S_{44})(l_1{}^2 l_2{}^2 + l_2{}^2 l_3{}^2 + l_1{}^2 l_3{}^2)\}^{-1} \quad (5)$$

where the l_i are the direction cosines for the vector l and S_{mn} are the compliance elements. For monocrystalline silicon the compliance elements are S_{11}=7.68x10^{-12}Pa, S_{12}=-2.14x10^{-12}Pa and S_{44}=12.6x10^{-12}Pa, (Wortman and Evans, 1965).

3.3. Second Moment of Area

In order to compute the second moment of area of the beams with hexagonal cross section, the hexagon was divided in basic components, four triangle and four square, whose the equivalent moment of area can be easily calculated by,

$$I = \frac{(2\sqrt{2}\,t_b + 4w_b){t_b}^3}{48} \quad (6)$$

3.4. Effective Mass

The accelerometer's seismic mass with the geometric form described previously can be obtained by,

$$M_s = \rho_{Si}\,({W_m}^2\,T_m + \frac{\sqrt{2}}{2} W_m\,{T_m}^2 + \frac{{T_m}^3}{6}) \quad (7)$$

where ρ_{Si} is the silicon density that in room temperature is equal to 2330kg/m^3, (Hull, 1999).

The effective mass of a clamped-clamped beam m_{bef} is obtained using the Rayleigh principle, (Rao, 2003),

$$m_{bef} = \frac{13}{35} m_b \quad (8)$$

The effective mass of the accelerometer can then be determined by,

$$M_{eff} = M_s + n\frac{13}{35} m_b \quad (9)$$

where n is the number of beams, in this case n is equal to 2, i.e., there are two clamped-clamped beam.

3.5. Equivalent damping coefficient for Small and Large Displacement

The air trapped inside the set of wafers acts as a damping system when the seismic mass moves up and down due to an external acceleration acting in the normal direction to the seismic mass surface.

The damping coefficient as a function of the pressure for a incompressible gas is given by the Modified Reynolds equation as (Bao and Yang, 2007),

$$b_d = \frac{\eta_o L_m {W_m}^3}{Q_{pr}(p){h_o}^3}\beta(\Gamma) \quad (10)$$

where η_o viscosity of air that in room temperature and ambient pressure is equal to 18.192 x 10^{-6} Pa.s, $\beta(\Gamma)$ is the geometrical correction factor that for a square plate is $\beta(W_m = L_m) = 0.4217$, Yeh and Najafi (1997).

The relative flow rate coefficient Q_{pr} is determined using Boltzmann's transport equation and it cannot be expressed in a closed form. Veijola *et. al.* (1995) derived the following approximation that differs by less than 5% from the original equation, Veijola *et. al.* (1998):

$$Q_{pr} = 1 + 9.638(\sigma_p K_n)^{1.159} \quad (11)$$

where K_n is the knudsen number and σ_p is the coefficient to include slip-flow effects given by:

$$\sigma_p = \frac{2 - \alpha_v}{\alpha_v}[1.016 - 0.1211(1 - \alpha_v)] \quad (12)$$

where α_v is the tangential momentum accommodation coefficient (TMAC) and it is defined as the fraction of molecules which are diffusively reflected. Experimental results show that silicon has TMAC of about 0.7 with several gases, Bao and Yang (2007) and Gad-el-Hak (2006).

The knudsen number is given by,

$$K_n = \frac{\lambda}{h_o} \quad (13)$$

where λ is the mean free path of gas which is function of the gas pressure, therefore the damping coefficient is also function of it.

The accelerometer described has a differential configuration, thus there is another thin film of gas between the moveable plate and the upper fixed plate (upper stationary electrode). The equivalent damping coefficient can be obtained by association of dampers, Peeters *et. al.* (1991). The large displacement was derived replacing the gap by the gap minus the displacement z,

$$b_d = \frac{\eta_o L_m {W_m}^3}{Q_{pr}(p){h_o}^3}\beta(\Gamma)\left[\frac{1}{(1 - z/h_o)^3} + \frac{1}{(1 + z/h_o)^3}\right] \quad (14)$$

3.6. Electric Force

The electric forces between the accelerometer's electrodes are taken into account by the difference between the electric energy stored in the upper and the lower capacitor, as show in Fig 3.

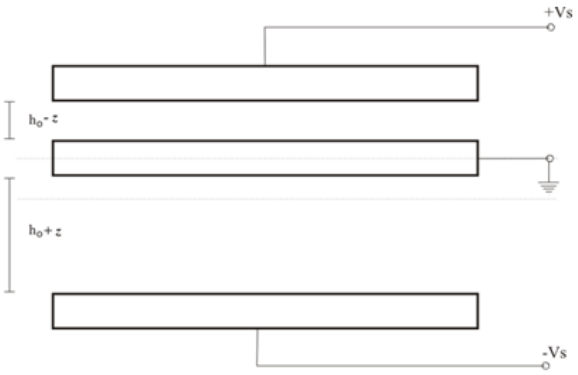

Figure 3. Differential capacitor with the inertial mass forms a moveable inner electrode.

The electric force equivalent is given by,

$$F_e = \frac{\varepsilon_r \varepsilon_o A_m V_s^2}{2}\left[\frac{1}{(h_o - z)^2} + \frac{1}{(h_o + z)^2}\right] \quad (15)$$

where ε_o is the vacuum permittivity, ε_r is the relative permittivity, A_m is the electrode area and Vs is the DC applied voltage, which in the model simulated is equal to 5V.

3.7. Nonlinear and Linear Dynamic Model

The dynamic model the microaccelerometer is obtained by the following governing equations of motion,

$$M_{eff} a_z = M_{eff}\frac{d^2 z}{dt^2} + \begin{Bmatrix} F_z(u) \\ \delta_z(u) \end{Bmatrix} z + \\ + \frac{\eta_o L_m {W_m}^3}{Q_{pr}(p){h_o}^3}\beta(\Gamma)\left[\frac{1}{(1 - z/h_o)^3} + \frac{1}{(1 + z/h_o)^3}\right]\frac{dz}{dt} + \\ - \frac{\varepsilon_r \varepsilon_o A_m V_s^2}{2}\left[\frac{1}{(h_o - z)^2} + \frac{1}{(h_o + z)^2}\right] \quad (16)$$

which is a nonlinear second order differential equation with time-varying coefficients. However, it can be linearized term by term using Taylor series expansion around the operation point z equal to zero,

$$M_{eff} a_z = M_{eff}\frac{d^2 z}{dt^2} + k_{eq} z + \frac{\eta_o L_m {W_m}^3}{Q_{pr}(p){h_o}^3}\beta(\Gamma)\frac{dz}{dt} + \\ - \frac{2\varepsilon_r \varepsilon_o A_m V_s^2}{{h_o}^3} z \quad (17)$$

4 Results and discussion

The silicon wafer used has orientation (100) and the primary flat is oriented in [110] direction. Accelerometer's beams that are parallel or perpendicular to flat have the same orientation. Young's modulus Eq. (5) to [110] direction are 168.9GPa.

The normalized deflection as a function of the force is shown in Fig. 4.

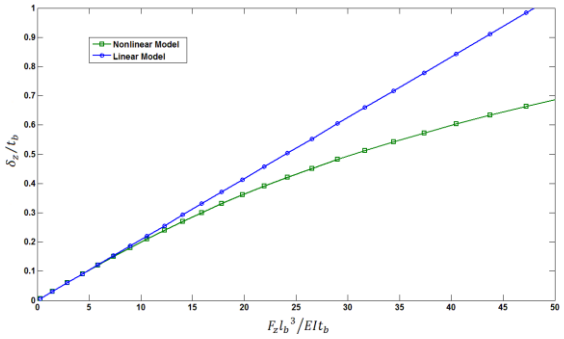

Figure 4. Comparison between the linear and nonlinear models of normalized deflection.

Figure 4 shows that the small deflection theory is valid for deflections up to roughly a quarter of the beam thickness. For deflections above this value large deflection theory has to be used. The beam thickness t_b is 55µm hence the small deflection theory is valid for deflections until 13.75µm.

Fig. 5 shows a comparison between the linear and nonlinear damping models using the data from Table 1.

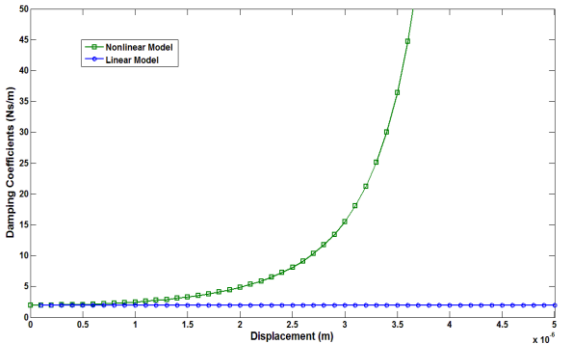

Figure 5. Comparison between the linear and nonlinear models of damping coefficients.

The graph in Fig. 5 shows that for a displacement of about 20% of the gap size, the models' results are practically the same. However, for larger displacement the model used starts to disagree with the small displacement model.

The nonlinear dynamic model Eq. (16) and a linearized model Eq. (17) were simulated using Simulink®. The Fig. 6 shows a comparison between the two models in function of the applied acceleration.

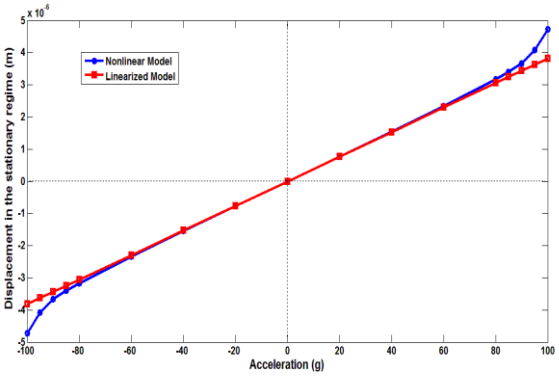

Figure 6. Nonlinear and linearized models versus acceleration.

The Fig. 6 shows that for small acceleration the linearized model can be used. However, for large acceleration values the nonlinear model has to be used.

Using the linearized model, the Eq. (10) was used to calculate the viscous damping coefficient with different pressure values. Considering silicon as the plates material and air as the gas between them, when the pressure p is equal to the ambient pressure, the relative flow rate coefficient is equal to 1.060.

The simulated results were obtained using the 3D model and the commercial software COMSOL Multiphysics®. This software has the modified Reynolds equation as part of its CFD package, COMSOL (2010). The simulations were done using PC with an Intel® Core™ i7 processor, 4GB Dual Channel DDR3 SDRAM memory and 500GB (5400RPM) Hard-Drive. The solution time was about 7 hours for each value of pressure, using a tetrahedral mesh with 38,701 elements.

The Fig. 7 shows a comparison between the analytical and the CFD results for step input of 1g.

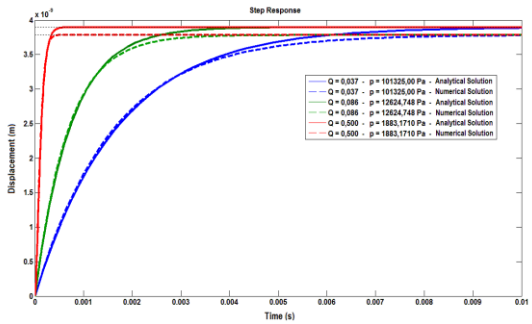

Figure 7. Analytical and CFD time response for step input of 1g.

The simulations were done for tree different pressure values. The pressure values are 10^3Pa, 10^4Pa and the ambient pressure which leads a knudsen numbers of 0.006823, 0.06913 and 0.69 and the relative flow rate coefficients of 1.060, 1.872 and 13.570, respectively. Fig. 7 shows the system changing from an under-damper system into an over-damped system.

Fig. 7 also shows that the analytical results in the time-domain are in agreement with the CFD results and it represents perfectly the three characteristics of the system: under-damping, critically-damped and over-damped. There is a little difference of 4% in the amplitude between the analytical and the CFD results, however the settling times are approximately the same.

The following figures show the comparison between the results in the frequency-domain for different pressure values. The amplitude response as a function of the frequency is shown in Fig. 8 and the phase response is shown in Fig. 9. These figures show that the analytical results in the frequency - domain are in very good agreement with the CFD ones. The small difference observed at amplitude in the time domain response is not observed anymore in the frequency domain, due to the fact that it takes into account the normalized amplitude.

It is well known that for a classical oscillator with linear damping, a maximum bandwidth is attained when a damping ratio of 0.7 is set. Therefore, with the damping coefficient is possible to calculate the exactly pressure that leads this damping ratio. However, it is important to highlight that when one works with pressure bellow the ambient pressure in microscale, some of the vacuum issues, as for example gas leaks, become a big problem.

As can be seen in Eq. (10) the damping coefficient is highly dependent on the gap size, i.e., the bandwidth optimization also can be done by controlling the gap size. However, in capacitive accelerometers the gap size has a fundamental importance from the electrical point of view, so it has not a free range. Another way to control damping is through perforations in the plate; however it increases the micromachining process complexity.

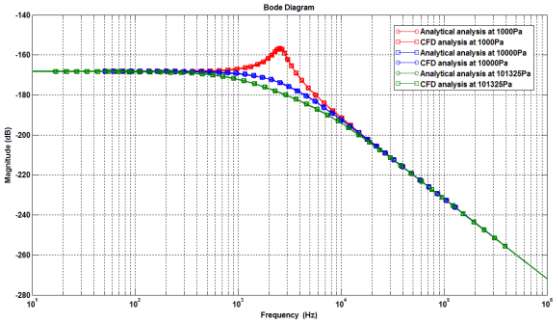

Figure 8. Analytical and CFD results to magnitude versus frequency.

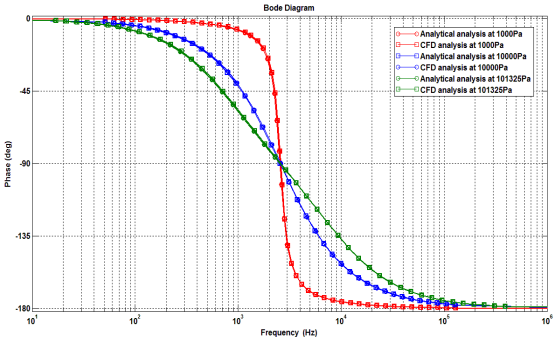

Figure 9. Analytical and CFD results of phase versus frequency.

5 Conclusions

The accurate determination of the dynamic model is of great technological importance to characterization and optimization of the inertial microdevices.

The results obtained in this work by applying the analytical model presented for damping analysis of a differential capacitive accelerometer are quite accurate when compared with the CFD results. Moreover, as expected, solving the problem by applying the analytical model is much faster than obtaining the CFD solutions.

DOI: 10.5540/03.2013.001.01.0140

The analytical results can be applied now to study the dynamic behavior of the bulk-micromachined accelerometer in the closed loop configuration.

Acknowledgements

This work was supported by FINEP (Brazilian Agency for Funding of Studies and Projects), under grant n: 01.09.0395.00, project ACELERAD.

References

Bao, M. and Yang, H., 2007, "Squeeze film air damping in MEMS", Sensor and Actuators A, Vol. 136, pp. 3–27. DOI: 10.1016/j.sna.2007.01.008

Beer, F. P., Johnston, E. R. and DeWolf, J. T., 2006, "Mechanics of Materials" Ed. McGraw-Hill, New York, USA, Vol. 4, 400 p.

Brantley, W. A., 1973, "Calculated elastic constants for stress problems associated with semiconductor devices", Journal of Applied Physics, Vol. 44, pp. 534–535. DOI: 10.1063/1.1661935

COMSOL Multiphysics, 2010, "Squeeze-Film Gas Damping in an Accelerometer", COMSOL user's manual.

Dziuban, J.A., 2006, "Bonding in Microsystem Technology", Ed. Springer, Netherlands, 331 p.

Gad-el-Hak, M., 2006, "The MEMS Handbook", Ed. CRC Taylor & Francis, New York, USA, 200 p.

Hull, R., 1999, "Properties of Crystalline Silicon", Ed. INSPEC, London, UK, Vol. 20, 1042 p.

Legtenberg, R., Groeneveld, A. W. and Elwenspoek, M., 1996, "Comb-drive Actuator for Large Displacements", Journal of Micromechanics and Microengineering, Vol. 6, pp. 320–329. DOI: 10.1088/0960-1317/6/3/004

MNX, 2008. "MEMS and Nanotechnology Applications" MEMS & Nanotechnology Exchange. 5 Jan. 2011 <http://www.memsnet.org/mems/applications.html>.

Peeters, E., Vergote, S., Puers, B. and Sansen, W., 1991, "A Highly Symmetrical Capacitive Micro-Accelerometer With Single Degree-of-Freedom Response", Proceedings of the 6th International Conference Solid-State Sensors and Actuators (Transducers' 91), San Francisco, CA, USA, June 24-28, pp 97-100.

Rao, S. S., 2003, "Mechanics of Materials" Ed. Prentice Hall, New York, USA, Vol. 4, 1078 p.

Wortman, J. J., and Evans, R. A., 1965, "Young's Modulus and Poisson's Ratio in Silicon and Germanium", Journal of Applied Physics, Vol. 36, pp. 153–156. DOI: 10.1063/1.1713863

Veijola, T., Kuisma, H., Lahdenpara, J. and Ryhanen, T., 1995, "Equivalent-Circuit Model of Squeezed Gas in a Silicon Accelerometer", Sensor and Actuators A, Vol. 48, pp. 239–248. DOI: 10.1016/0924-4247(95)00995-7

Veijola, T., Kuisma, and Lahdenpara, J., 1998, "The Influence of Gas-Surface Interaction on Gas-Film Damping in a Silicon Accelerometer", Sensor and Actuators A, Vol. 66, pp. 83–92. DOI: 10.1016/S0924-4247(97)01732-9

Yeh, C. and Najifi, K., 1997, "A Low-Voltage Tunneling-Based Silicon Microaccelerometer", IEEE Transaction on Electron Devices, Vol. 44, Nº11, pp. 1875–1882 DOI: 10.1109/16.641355

